Oxygen atom transfer using an iron(IV)-oxo embedded in a tetracyclic N-heterocyclic carbene system: How does the reactivity compare to Cytochrome P450 Compound?

DOI:
10.1002/chem.201605505

Document Version
Accepted author manuscript

Oxygen atom transfer using an iron(IV)-oxo embedded in a tetracyclic N-heterocyclic carbene system: How does the reactivity compare to Cytochrome P450 Compound?

Fabián G. Cantú Reinhard,[a] and Sam P. de Visser*[a]

Abstract: N-heterocyclic carbenes (NHC) are common catalyst features in transition metal chemistry. Recently, a cyclic system containing four NHC groups with a central iron atom was synthesized and its iron(IV)-oxo characterized, $[Fe^{IV}(O)(cNHC_4)]^{2+}$. This tetra-cyclic NHC ligand system may give the iron(IV)-oxo species unique catalytic properties as compared to traditional nonheme iron and heme iron ligand systems. Therefore, we performed a computational study on the structure and reactivity of the $[Fe^{IV}(O)(cNHC_4)]^{2+}$ complex in substrate hydroxylation and epoxidation reactions. The reactivity patterns are compared with cytochrome P450 Compound I and nonheme iron(IV)-oxo models and it is shown that the $[Fe^{IV}(O)(cNHC_4)]^{2+}$ system is an effective oxidant with oxidative power analogous to P450 Compound I. Unfortunately, in polar solvents a solvent molecule will bind to the sixth ligand position and decrease the catalytic activity of the oxidant. A molecular orbital and valence bond analysis provides insight into the origin of the reactivity differences and makes predictions on how to further exploit these systems in chemical catalysis.

Introduction

Heme enzymes are versatile catalysts in nature and come in a large variety of shapes and structures that give them their unique biochemical functions. For instance, the heme peroxidases and catalases detoxify the body from hydrogen peroxide,[1,2] while the cytochromes P450 typically react as monoxygenases through oxygen atom transfer with substrates as a means to initiate the metabolism of drugs, the biodegradation of xenobiotics as well as the biosynthesis of hormones.[3] Heme peroxidases, catalases and monoxygenases have in common that they generate a high-valent iron(IV)-oxo heme cation radical species, called Compound I (CpdI).[4] CpdI is highly reactive, but nevertheless, has been characterized in several peroxidases using a range of spectroscopic techniques, including electron paramagnetic resonance, Mössbauer and UV-Vis absorption spectroscopies.[5] In P450 chemistry, CpdI has been more challenging to trap and characterize but spectroscopic studies of Rittle and Green provided evidence on its existence. Moreover, it was shown to be in a doublet spin ground state with two unpaired electrons in π^*_{FeO} orbitals and a third unpaired electron in a heme-thiolate type orbital called a_{2u}.[6] The difference in reactivity of peroxidases and monoxygenases was assigned to the axial ligand bound to the metal (trans to the oxo group in CpdI), which is typically cysteinate in the P450s but histidine in peroxidases.[7]

Over the years, a large number of synthetic model complexes that resemble the active site of heme enzymes have been created with the aim to gain insight into the characteristic properties of metal and ligand on structure and reactivity.[8] In particular, oxidants were created with heme-analogues, such as corrole, corrolazine and phthalocyanine,[9–11] which have differences in their aromaticity, overall charge and electron-donating/withdrawing properties. These studies have given insight into the function and properties of the heme and how it influences reaction mechanisms and spectroscopic variables. For instance, corroles and corrolazines have an overall charge of 3– and as such can stabilize metals in high oxidation states.

One specific structural feature that is commonly used in catalysis nowadays are the N-heterocyclic carbenes (NHC).[12] Very recently, Kühn and co-workers synthesized and characterized a tetra-cyclic NHC complex ($cNHC_4$), whereby the four NHC components were bridged by alkyl groups.[13] Its geometry and, in particular the one with bridging methyl groups as is studied here, shows structural similarity to a porphyrin (Por) manifold, see Scheme 1, although it misses the strong π-conjugation. Clearly, the $cNHC_4$ ligand is tetradentate like porphyrin, but lacks the large conjugated π-system characteristic for its absorption spectrum and responsible for electron abstraction during monoxygenation reactions. Recent studies of Meyer and co-workers spectroscopically characterized an iron(IV)-oxo species with the $cNHC_4$ ligand system and showed it to be in a triplet spin ground state.[14] So far little is known on the catalytic properties of this tetra-cyclic NHC complex and no studies on reactivity patterns have been reported. In particular, the tetra-cyclic NHC chemical system may have catalytic properties unrivalled to in nonheme iron chemistry. To find out whether the iron(IV)-oxo species with tetra-cyclic NHC ligand would potentially be an active oxidant of oxygen atom transfer reactions we decided to do a detailed density functional theory (DFT) study. In particular, we compare two iron(IV)-oxo complexes, namely with $cNHC_4$ or Por ligand system, i.e. $[Fe^{IV}(O)(cNHC_4)X]^{2+}$ with X = no ligand or CH_3CN and $[Fe^{IV}(O)(Por)(SH)]$ as a model of P450 CpdI. We hypothesized that the electron donation of the NHC groups toward iron, may affect the electron affinity of the complex and consequently its reactivity patterns with substrates. We initially investigated the iron(IV)-oxo complex with $cNHC_4$ ligand system with and without an axial solvent (acetonitrile) ligand. Thereafter, we studied the reactivity patterns for oxygen atom transfer and calculated double bond epoxidation of styrene and propene and aliphatic hydroxylation of propene and ethylbenzene (Scheme 1).

[a] F.G. Cantú Reinhard, Dr S.P. de Visser
Manchester Institute of Biotechnology and School of Chemical Engineering and Analytical Science
The University of Manchester, 131 Princess Street,
Manchester M1 7DN, United Kingdom
sam.devisser@manchester.ac.uk

Supporting information for this article is given via a link at the end of the document.

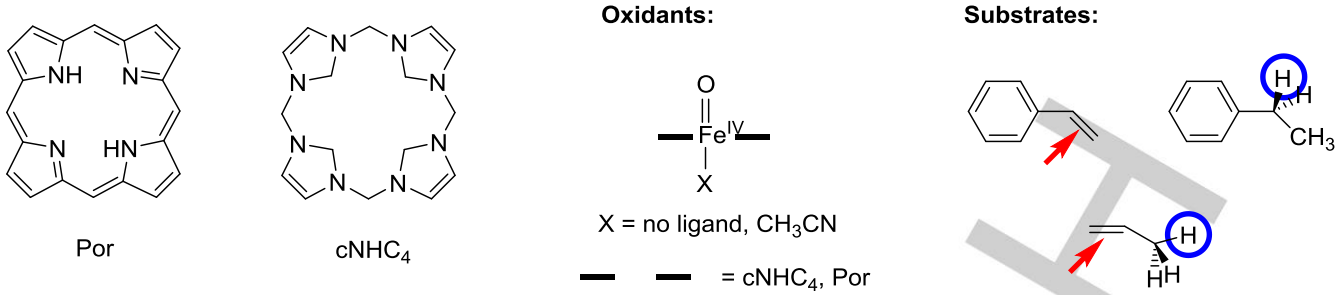

Scheme 1. Oxidants and substrates studied in this work.

The studies here are compared to previous work on iron(IV)-oxo porphyrin systems[15] and nonheme iron(IV)-oxo models and shows that the $[Fe^{IV}(O)(cNHC_4)]^{2+}$ oxidant is a good oxidant that reacts with comparable rate constants as $[Fe^{IV}(O)(Por)(SH)]$ system, however, in acetonitrile a solvent molecule will bind the sixth ligand position and reduce its catalytic activity.

Results

Our work started off with a detailed analysis of the structure and spectroscopic properties of $[Fe^{IV}(O)(cNHC_4)]^{2+}$ (^{3,5}**1**) and $[Fe^{IV}(O)(cNHC_4)(CH_3CN)]^{2+}$ (^{3,5}**1**$_{AN}$), whereby the latter contains a solvent acetonitrile molecule in the sixth ligand position trans to the oxo group. We initially did a gas-phase geometry optimization, but later redid the work with an implicit solvent model with a dielectric constant mimicking acetonitrile, as recent studies showed this to give a better match to experimental free energies of activation.[16] Here we will focus on the solvent optimized geometries, whereas gas-phase results can be found in the Supporting Information. Typically for nonheme iron(IV)-oxo complexes there are two close-lying spin states, namely the triplet and quintet spin states, and dependent on the ligand environment and solvent their ordering can change.[17] Our model uses methyl bridges between the four NHC groups and optimized geometries of $[Fe^{IV}(O)(cNHC_4)]^{2+}$ (**1**) and $[Fe^{IV}(O)(cNHC_4)(CH_3CN)]^{2+}$ (**1**$_{AN}$) are given in Figure 1. In the quintet spin state the axial acetonitrile molecule displaces itself from the iron(IV)-oxo species and hence no stable ^{5}**1**$_{AN}$ structure can be formed and acetonitrile (or alternative neutral molecules) will not bind in the axial position in the quintet spin state. This is most probably due to occupation of the σ^*_{z2} orbital with one electron that creates extra antibonding interactions along the O–Fe–axial ligand axis and prevents acetonitrile from binding. The Fe–O bond lengths are around 1.62 – 1.64 Å in the triplet spin state, which are values in good agreement with previous experimental and computational studies of nonheme iron(IV)-oxo complexes.[18,19] While our study was under consideration, Neese et al[14], reported an experimental report on an iron(IV)-oxo complex with tetra-cyclic NHC complex; however, their model had two bridging methyl and ethyl groups (designated complex **2**) rather than the four methyl linkages between the NHC groups as used here. The change in ligand system reduces the Fe–O distances by about 0.01Å and, consequently will affect vibrational frequencies slightly. Specifically, the two ethyl linkages used in Ref [14] create a stronger saddling than that seen in the structures in Figure 1. Despite this, there is still considerable saddling seen in the geometries with respect to a planar porphyrin ring. In particular, the two meso-methyl carbon atoms are below the iron(IV) atom as measured along the line through the iron(IV)-oxo by more than 1Å, while the other two meso-carbon atoms are located above the position of the iron atom by +0.58Å in ^{3}**1** and by +0.76Å in ^{3}**1**$_{AN}$. Therefore, the saddling on the side of the iron(IV)-oxo group is less than that on the axial ligand side.

In structure **1**, the triplet spin state is the ground state and well separated from the quintet spin state by ΔE+ZPE = 15.1 kcal mol^{-1}. This energy gap is considerably larger than that typically found for iron(IV)-oxo porphyrins and nonheme iron(IV)-oxo models.[20,21] In particular, the latter tends to have a high-spin ground state with pentacoordinated ligands, while the triplet spin state is lower in energy in hexacoordinated environments. The group spin densities are given in Figure 1 and show one unpaired electron on the iron and oxo groups in the triplet spin state, although there is a small polarization toward iron radical in both cases. Very little spin density is seen on the $cNHC_4$ ligand. As the $[Fe^{IV}(O)(cNHC)_4]^{2+}$ complex, either with or without axial ligand has clearly separated triplet and quintet spin state surfaces, it makes the complex highly suitable for understanding triplet spin reactivity. In particular, since some computational studies have suggested that nonheme iron(IV)-oxo reactivity proceeds on a dominant quintet spin state, while the triplet spin surface shows sluggish reactivity.

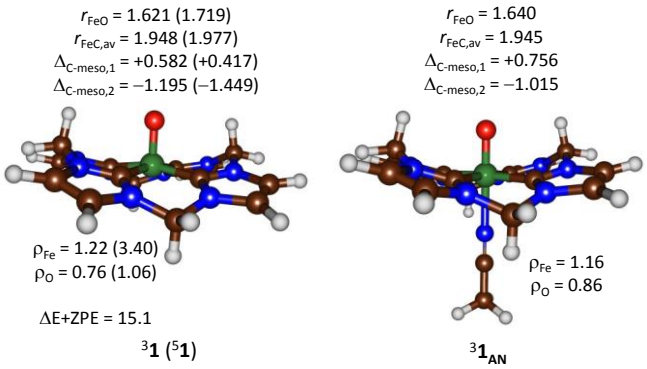

Figure 1. Optimized geometries (UB3LYP+PCM) of iron(IV)-oxo complexes with $cNHC_4$ ligand system. Bond lengths are given in angstroms, group spin densities (ρ) in atomic units and relative energies in kcal mol^{-1}. The saddling was estimated from the displacement of the meso-carbon with respect to the iron atom ($\Delta_{C\text{-}meso}$).

Subsequently, we analyzed the molecular orbitals of ^{3}**1** in detail, see Figure 2. As commonly seen in iron(IV)-oxo complexes the

Fe–O interaction is described by a pair of π_{xz}/π^*_{xz} and π_{yz}/π^*_{yz} orbitals due to the interaction of the $3d_{xz}/3d_{yz}$ atomic orbital on iron with a $2p_x/2p_y$ orbital on oxygen. The bonding pairs are doubly occupied, while the antibonding pairs are singly occupied. In addition, there is one σ-type orbital along the Fe–O bond, i.e. $\sigma_{z2}/\sigma^*_{z2}$, for the interaction of the iron $3d_{z2}$ with the $2p_z$ on oxygen and the bonding combination is filled, whereas the antibonding is high in energy and virtual. The same is the case for the $\sigma_{x2-y2}/\sigma^*_{x2-y2}$ pair of orbitals that represent the bonding and antibonding interactions of the metal with the four carbon atoms of the NHC groups. The final set of orbitals highlighted in Figure 2 are the carbene orbitals of the NHC ligands that give the $\sigma_{d,xz}/\sigma_{d,yz}$ orbitals highlighted. Therefore, the electronic configuration of ^{3}**1**/^{3}**1**$_{AN}$ is $\pi^*_{xy}{}^2\ \pi^*_{xz}{}^1\ \pi^*_{yz}{}^1$, whereas it is $\pi^*_{xy}{}^1\ \pi^*_{xz}{}^1\ \pi^*_{yz}{}^1\ \sigma^*_{z2}{}^1$ for ^{5}**1**/^{5}**1**$_{AN}$.

As can be seen from Figure 2, there is a considerable energy gap for the α-set of orbitals between the π^*_{xz}/π^*_{yz} orbitals on the one hand, with the σ^*_{z2} orbital on the other hand. This large separation of the π* and σ* orbitals stabilizes the triplet spin state over the quintet spin state in energy. Indeed, a large triplet-quintet energy gap of larger than 15 kcal mol^{-1} is reported above in Figure 1. Furthermore, a large HOMO-LUMO gap may implicate a large electron affinity and hence sluggish reactivity with substrates as proposed previously.[22] Details of the reactivity patterns and a thermochemical analysis of the oxidative properties of the iron(IV)-oxo species will be discussed in detail below.

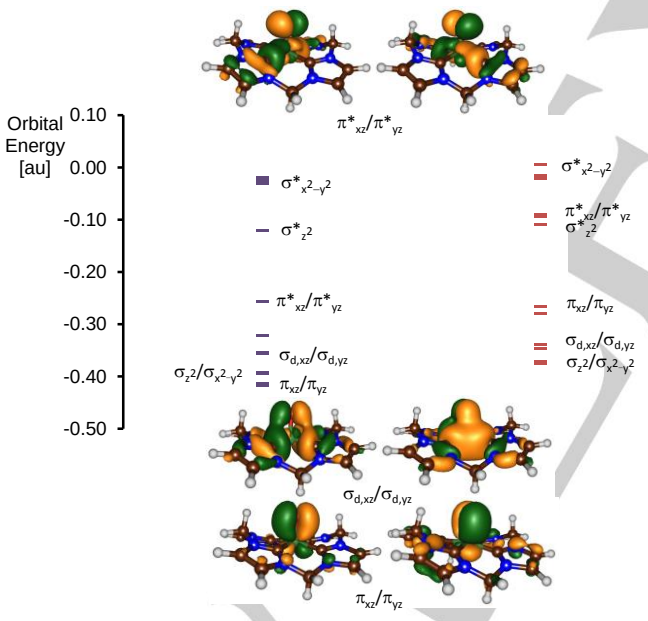

Figure 2. Orbital energy diagram of ^{3}**1** as obtained at B3LYP/BS2.

Subsequently, we investigated the effect of the alkyl bridge of the tetracyclic NHC iron(IV)-oxo complexes and compared the system from this work with the one from Neese et al.[14] In particular, we calculated spectroscopic parameters for complexes ^{3}**1** and ^{3}**2**, whereby both are iron(IV)-oxo complexes with tetracyclic NHC ligand system, but **1** has four methyl bridges and **2** has two ethyl and two methyl bridges. Firstly, the extension of the bridges from methyl to ethyl has very limited effect on the Fe–O frequency, and values of 959 cm^{-1} for ^{3}**1** and 961 cm^{-1} for ^{3}**2** (B3LYP/BS1+PCM optimized geometry) are found. By contrast, optimized geometries for the acetonitrile ligated complexes, at the same level of theory, are 928 cm^{-1} for ^{3}**1**$_{AN}$ and 933 cm^{-1} for ^{3}**2**$_{AN}$. Therefore, addition of an acetonitrile molecule to the sixth ligand position leads to a major drop in Fe–O frequency (by about 30 cm^{-1}) due to shortening of the Fe–O bond. On the other hand changing the alkyl bridge from methyl to ethyl has little effect on the Fe–O bond length and frequency.

To find out whether other spectroscopic variables are more strongly affected by the change in the NHC alkyl bridges, we calculated the Mössbauer parameters of ^{3}**1** and ^{3}**2**. Interestingly, the quadrupole splitting drops from ΔE_Q = 3.52 mm s^{-1} for ^{3}**1** to 2.72 mm s^{-1} for ^{3}**2**, respectively. As such, the ligand system influences some spectroscopic properties strongly, whereas other factors are lesser effected.

Next, we investigated the oxygen atom transfer ability of **1** and **1**$_{AN}$ with substrates and specifically double bond epoxidation and aliphatic C–H bond hydroxylation were studied. Firstly, we will discuss double bond epoxidation of styrene and propene and the lowest energy profile is shown in Figure 3. The triplet spin state is the ground state for this system and stays the lowest energy conformation throughout the full reaction mechanism. This is unique in iron(IV)-oxo chemistry as usually a spin state crossing from the triplet to the quintet spin state takes place. Nevertheless, the calculations presented here show that the triplet spin state can be reactive in substrate oxidation. The quintet spin state starts off above the triplet by 15 kcal mol^{-1} in the reactants and its surface, therefore, is inaccessible during the electrophilic attack that happens initially. Thus the iron(IV)-oxo attacks the terminal carbon atom via an electrophilic addition transition state **TS**$_E$ to form a radical intermediate **I**$_E$. The stepwise reaction continues with a ring-closure transition state **TS**$_{rc}$ to form the epoxide-ring and generates the product complexes **P**$_E$. In all cases, the rate determining step in the mechanism is the initial C–O bond formation barrier (**TS**$_E$), which is followed by a small ring-closure transition state.

The transition states (^{3}**TS**$_E$) are characterized with a large imaginary frequency of well over 500 cm^{-1}. These frequencies are in line with those found for substrate epoxidation by iron(IV)-oxo porphyrin and nonheme complexes that gave values typically between *i*250 – *i*500 cm^{-1}.[23] It was shown that for a set of para-substituted styrene systems, the barrier height for substrate epoxidation correlated with the imaginary frequency in the transition state,[24] whereby large imaginary frequencies correlated with relative high activation energies for substrate epoxidation. Nevertheless, as discussed in detail later, the barrier heights for styrene and propene double bond activation by ^{3}**1** are similar to those found for a P450 Compound I model.

Structures are typical for substrate epoxidation reactions and see an elongation of the Fe–O bond due to occupation of the σ^*_{z2} orbital with one electron. Thus, the electrophilic pathway via **TS**$_E$ results in an electron transfer from substrate to iron(IV)-oxo species that occupies the virtual σ^*_{z2} orbital with one electron. This, so-called $^3\sigma$-pathway,[25] gives an iron(III) intermediate (^{3}**I**$_E$) with orbital occupation with three unpaired electrons with up-spin on the metal ($\pi^*_{xz}{}^1\ \pi^*_{yz}{}^1\ \sigma^*_{z2}{}^1$) and a down-spin radical on the carbon atom of the substrate ($\phi_{Sub}{}^1$). Group spin densities (see Supporting Information) confirm the assigned pathway.

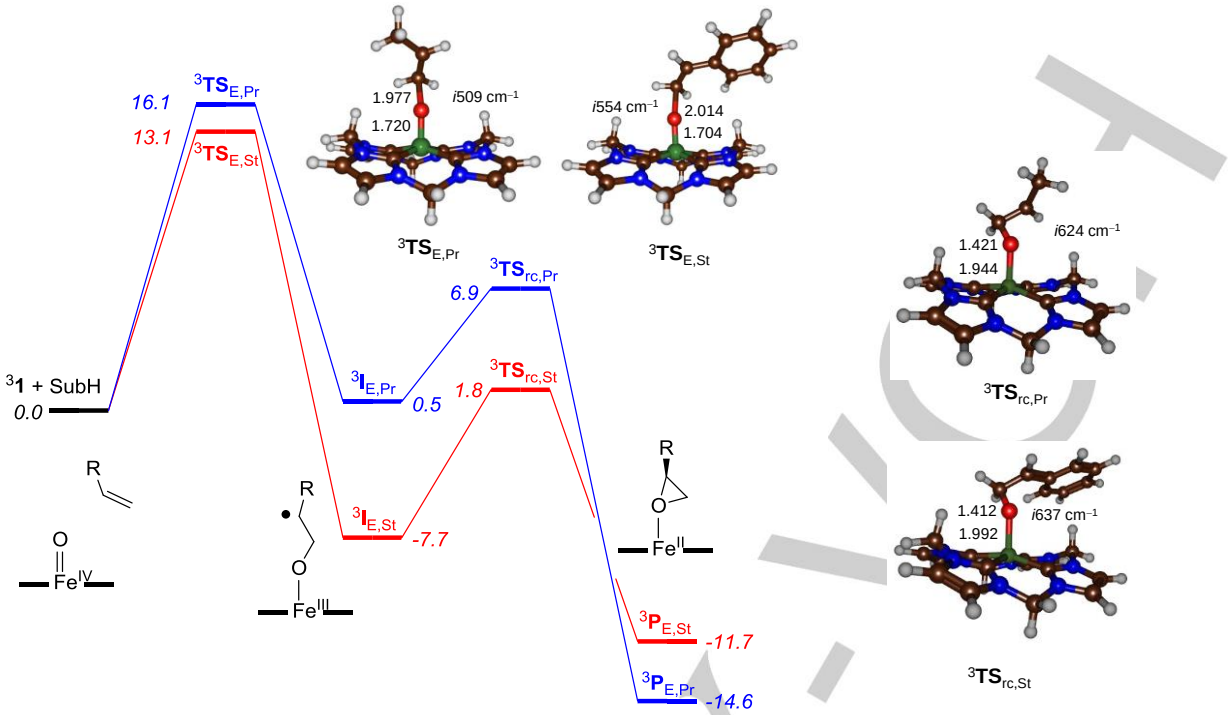

Figure 3. Potential energy surface and rate determining transition state geometries for styrene (St) and propene (Pr) epoxidation by ^{3}**1** as calculated at UB3LYP/BS2+PCM//UB3LYP/BS1+PCM. Bond lengths are given in angstroms, the imaginary frequency is in cm^{-1} and relative energies (ΔE+ZPE+E$_{solv}$) in kcal mol^{-1}.

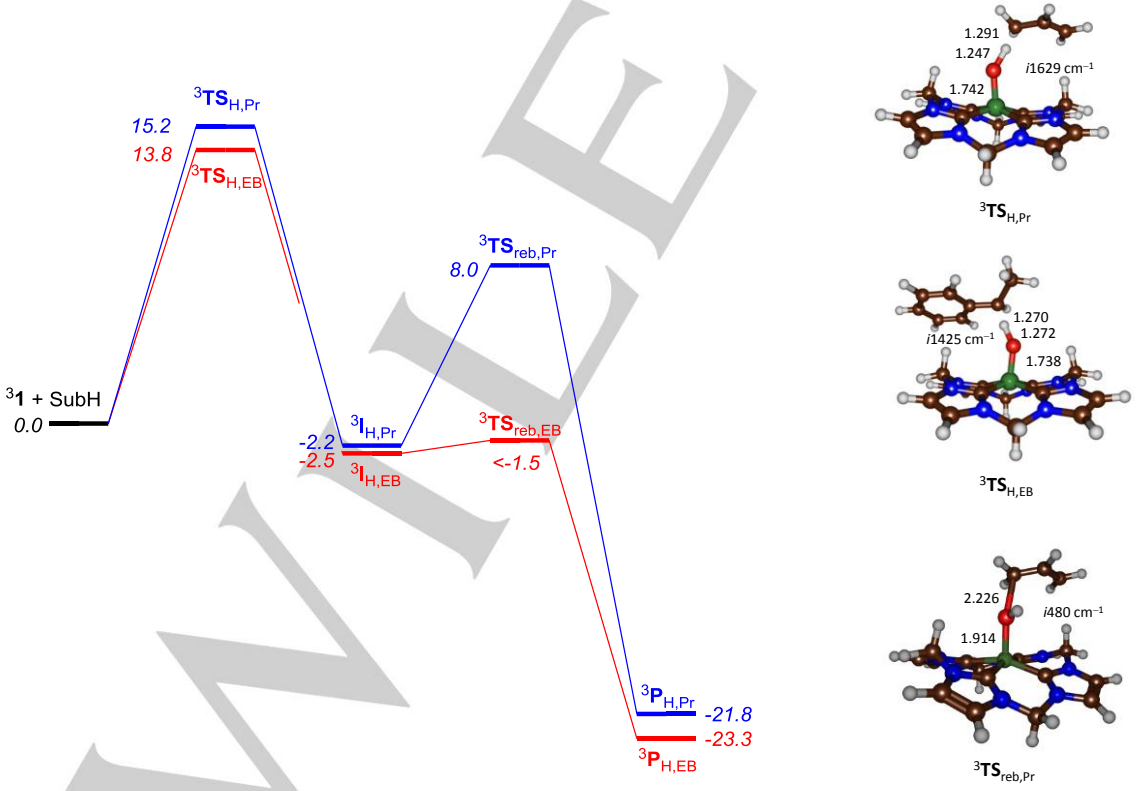

Figure 4. Potential energy surface and rate determining transition state geometries for ethylbenzene (EB) and propene (Pr) hydroxylation by ^{3}**1** as calculated at UB3LYP/BS2+PCM//UB3LYP/BS1+PCM. Bond lengths are given in angstroms, the imaginary frequency is in cm^{-1} and relative energies (ΔE+ZPE+E$_{solv}$) in kcal mol^{-1}.

The alternative pathway, i.e. the $^3\pi$-pathway, whereby the substrate donates an electron in the π^*_{xz} orbital instead gives a radical intermediate $^3\mathbf{I}_E$' with occupation $\pi^{*1}_{xz}\ \pi^{*1}_{yz}\ \sigma^{*0}_{z2}\ \phi^1_{Sub}$. However, for propene epoxidation we find the $^3\mathbf{I}_E$' state to be higher in energy by 10.6 kcal mol^{-1} than $^3\mathbf{I}_E$ and hence did not pursue this mechanism further.

Geometrically, the electrophilic transition states have elongated Fe–O bonds of about 1.720 / 1.704 Å for $^3\mathbf{TS}_{E,Pr}$ / $^3\mathbf{TS}_{E,St}$, respectively, whereas the reactant structure had a distance of 1.621 Å. At the same time, the substrate approaches the oxidant under a large angle Fe–O–C of 141° / 147° in $^3\mathbf{TS}_{E,Pr}$ / $^3\mathbf{TS}_{E,St}$. These angles are considerably larger than those found for typical $^3\pi$-pathways that tend to give an Fe–O–C angle of about 120° instead.[26] Most likely, these enlarged angles are a consequence of the non-planarity of the $cNHC_4$ ligand, so that the substrate cannot approach the iron(IV)-oxo under an ideal angle as a result of electronic repulsions with the ligand

After the electrophilic transition state the system relaxes to a radical intermediate ($^3\mathbf{I}_E$), which is separated from products via a ring-closure transition state ($^3\mathbf{TS}_{rc}$). The electron transfer from substrate to oxidant that happens in this reaction step fills the π^*_{xz} molecular orbital with a second electron, which reduces the spin density on iron and creates an iron(II) product complex with $\pi^{*2}_{xz}\ \pi^{*1}_{xz}\ \sigma^{*1}_{z2}$ orbital occupation. Optimized geometries of the ring-closure transition states are given in Figure 3. Now the bond between iron and oxo is broken and the oxygen atom inserts itself into the C–C bond to form the epoxide product. Hence, short O–C and long Fe–O distances are seen in both transition states.

The ring-closure barriers are relatively large (6.4 and 9.5 kcal mol^{-1} for propene and styrene, respectively), which implies that the radical intermediates will have a finite lifetime during which rearrangement process may occur leading, for instance, to stereochemical scrambling and the formation of cis-products from trans-reactants. In addition, side products leading to aldehydes or suicidal products in P450 chemistry of olefins were explained as originating from the lifetime of the radical intermediates.[27] Nevertheless, in all cases the barrier $\mathbf{TS}_E$ is rate determining.

Subsequently, we investigated the aliphatic hydroxylation pathways of two model substrates, namely ethylbenzene (EB) and propene (Pr) and the results are given in Figure 4. Similarly to the epoxidation mechanisms the reactions are stepwise via a radical intermediate ($\mathbf{I}_H$) and consist of a hydrogen atom abstraction via transition state $\mathbf{TS}_H$. The OH rebound step via transition state $\mathbf{TS}_{reb}$ gives the iron(III)-alcohol product complex $\mathbf{P}_H$. Again the rate-determining step is the initial barrier and the rebound barrier is smaller. Interestingly, we could not locate a rebound transition state for ethylbenzene hydroxylation, but for propene a considerable barrier of 10.2 kcal mol^{-1} was found.

Geometrically, both hydrogen atom abstraction barriers are central with almost equal C–H and O–H distances that displays a large imaginary frequency of well over i1400 cm^{-1}. An imaginary frequency of that magnitude will lead to a large kinetic isotope effect as a result of replacing the transferring hydrogen atom by deuterium. Indeed, we calculate an Eyring kinetic isotope effect (KIE_E) for hydrogen atom abstraction from propene and ethylbenzene of 6.6 and 6.7, respectively, whereas Wigner corrections due to tunneling raise these values to 9.3 and 9.1. These values match calculated and experimentally measured KIEs for hydrogen atom abstraction by nonheme iron(IV)-oxo and P450 Compound I models excellently.[28,29]

Similarly as the substrate epoxidation pathways, the radical intermediates $^3\mathbf{I}_H$ are characterized with an orbital occupation of $\pi^{*1}_{xz}\ \pi^{*1}_{yz}\ \sigma^{*1}_{z2}\ \phi^1_{Sub}$ as typical for $^3\sigma$-pathways. Indeed, the Fe–O distance in the $^3\mathbf{TS}_H$ structures is very similar to those in the $^3\mathbf{TS}_E$ geometries and so are the group spin densities. Formation of the radical intermediates is slightly exothermic by 2.2 and 2.5 kcal mol^{-1} for propene and ethylbenzene. Under these conditions, it appears that $^3[Fe^{IV}(O)(cNHC_4)]^{2+}$ should be able to react with olefins and aliphatic groups through substrate epoxidation and hydroxylation reactions.

Next, the styrene and propene epoxidation pathways were calculated for a series of different oxidants and the results are summarized in Table 1. First, an axial acetonitrile molecule was added to $^3\mathbf{1}$ to give $^3\mathbf{1}_{AN}$. Second, the tetra-cyclic NHC iron(IV)-oxo complex $^3\mathbf{2}_{AN}$ with two ethyl and two methyl linkages from Meyer et al[14] was studied. Thirdly, a heme and nonheme iron(IV)-oxo species were investigated, namely a small model of cytochrome P450 Compound I, ^{4}[Fe(O)(Por$^{+\bullet}$)(SH)],[30] and a typical nonheme iron(IV)-oxo with pentadentate ligand system N4Py (N4Py = *N*,*N*-bis(2-pyridylmethyl)-*N*-bis(2-pyridyl) methylamine) were studied.[31]

Table 1. Barrier heights $\mathbf{TS}_E$ for styrene and propene epoxidation by various iron(IV)-oxo complexes.

Oxidant	$\Delta E+ZPE+E_{solv}$[a]	Imag[b]	R(C–O)[c]	R(Fe–O)[c]
Styrene:				
$^3\mathbf{1}$	13.1	i554	2.014	1.704
$^3\mathbf{1}_{AN}$ ($^3\mathbf{2}_{AN}$)	20.7 (25.1)	i521	1.957	1.732
^{4}[Fe(O)(Por$^{+\bullet}$)(SH)]	12.4	i543	2.040	1.687
^{3}[Fe(O)(N4Py)]$^{2+}$	15.7	i448	1.999	1.714
Propene:				
$^3\mathbf{1}$	16.1	i509	1.977	1.720
$^3\mathbf{1}_{AN}$ ($^3\mathbf{2}_{AN}$)	22.8 (23.1)	i627	1.897	1.742
^{4}[Fe(O)(Por$^{+\bullet}$)(SH)]	17.1	i558	1.941	1.726
^{3}[Fe(O)(N4Py)]$^{2+}$	19.2	i493	1.981	1.720

[a] Values in kcal mol^{-1} calculated at UB3LYP/BS2+PCM//UB3LYP/BS1+PCM for complex $\mathbf{1}/\mathbf{1}_{AN}$ and UB3LYP/BS2+PCM//UB3LYP/BS1 for $\mathbf{2}_{AN}$. [b] Imaginary frequency in cm^{-1}. [c] C–O and Fe–O distances in angstroms.

Addition of an axially ligated solvent molecule to the $cNHC_4$ complex $^3\mathbf{1}$ gives a considerable rise of the transition state energies by more than 7 kcal mol^{-1}. The same is found for hydrogen atom abstraction from propene by $^3\mathbf{1}$ and $^3\mathbf{1}_{AN}$, which give $^3\mathbf{TS}_H$ barriers of 13.2 and 21.2 kcal mol^{-1}, respectively. This is similar to what was observed recently in μ-nitrido bridged diiron porphyrin and phthalocyanine complexes that gave much higher hydrogen atom abstraction barriers with an axially ligated anion at more than 5Å from the active oxo group.[32] As shown above in Figure 1 the iron atom is closer to the plane through the four carbene atoms, which destabilizes the π^* orbitals and makes the electron transfer into the metal-oxo group lesser

favorable. Therefore, complex ^{3}**1** in an acetonitrile solution will pick up a solvent molecule to form ^{3}**1**$_{AN}$. The resulting complex is a lesser good oxidant than ^{3}**1** for substrate epoxidation and hydroxylation reactions than the complex in the gas phase.

Complex ^{3}**1** actually gives enthalpies of activation of substrate epoxidation reactions that are close in energy to those found for P450 Compound I. For both propene and styrene the **TS**$_E$ barriers from ^{3}**1** and ^{4}[Fe(O)(Por$^{+\bullet}$)(SH)] are within 1 kcal mol^{-1}. As such, the N-heterocyclic carbene structure **1** is actually a very good oxidant. Unfortunately, in an acetonitrile solution ^{3}**1** will rapidly convert into ^{3}**1**$_{AN}$ and lose significant catalytic activity. Interestingly, ^{3}**1** is also better in activating propene and styrene than a typical iron(IV)-oxo oxidant, such as ^{3}[Fe^{IV}(O)(N4Py)]$^{2+}$, although axial binding of acetonitrile reverses the trend and ^{3}**1**$_{AN}$ reacts significantly slower than ^{3}[Fe^{IV}(O)(N4Py)]$^{2+}$.

For two substrates (styrene and propene), we also calculated the epoxidation transition state ^{3}**TS**$_E$ using the tetra-cyclic NHC complex with two bridging ethyl and two methyl groups, structure ^{3}**2**$_{AN}$. In the case of propene, the epoxidation barrier is within 0.3 kcal mol^{-1} of that obtained for ^{3}**1**$_{AN}$. However, for styrene the epoxidation barrier is raised by more than 4 kcal mol^{-1}, which may implicate that substrate approach is hindered due to the larger saddling in ^{3}**2**$_{AN}$ as compared to that of ^{3}**1**$_{AN}$. Previous studies on iron(IV)-oxo porphyrins showed that substrate epoxidation barriers are affected by ligands attached to the porphyrin scaffold and cause repulsive interactions that raise substrate activation barriers.[33]

Discussion

In the following, we will compare the aliphatic hydroxylation and olefin epoxidation reactions by ^{3}**1** and ^{3}**1**$_{AN}$ and particularly focus on the origins of the reactivity differences relative to those seen for analogous nonheme iron(IV)-oxo and iron(IV)-oxo porphyrin cation radical models. Let us first compare the effect of the environment, such as a polarized continuum model (PCM) and the addition of an axial ligand. Table 2 gives transition state (free) energies for styrene activation by ^{3}**1** and ^{3}**1**$_{AN}$ as calculated in the gas-phase and with a PCM model.

Table 2. Enthalpy of activation ($\Delta E^{\ddagger}$+ZPE) and Gibbs free energy of activation for styrene activation via **TS**$_{E,St}$.[a]

	$\Delta E^{\ddagger}$+ZPE		$\Delta G^{\ddagger}$	
Oxidant[a]	Gas-phase	PCM	Gas-phase	PCM
^{3}**1**	-1.0	13.1	9.9	23.9
^{3}**1**$_{AN}$	12.4	20.7	23.4	33.4

[a] Values obtained at UB3LYP/BS2//UB3LYP/BS1 in kcal mol^{-1}.

Similar to that seen before the free energy of activation is approximately 10 kcal mol^{-1} higher in value than the enthalpy of activation due to entropic effects with respect to isolated reactants.[34] Interestingly, a solvent model increases the barriers by 8.3 kcal mol^{-1} (for ^{3}**1**$_{AN}$) and 14.1 kcal mol^{-1} (for ^{3}**1**), which is probably the result of the charge of the chemical system, which is more polarized in the gas-phase. Furthermore, an axial ligand, such as a solvent molecule like acetonitrile, bound in the axial position of the iron(IV)-oxo complex raises the barriers drastically by 13.4 kcal mol^{-1}. This is in contrast to iron(IV)-oxo heme cation radical complexes, where the axial ligand is involved in key interactions to the metal and its electron-donating properties affect the electron affinity of the oxidant and consequently its oxygen atom transfer ability.[35]

These studies implicate that the ^{3}[Fe^{IV}(O)(cNHC$_4$)]$^{2+}$ will be an effective oxidant in the gas phase and probably apolar solvents, but becomes a significantly weaker oxidant in polar solvents that bind as sixth ligand to the complex. Nevertheless, a solvent molecule is only weakly bound to the iron(IV)-oxo complex and a binding strength of ΔE+ZPE+E$_{solv}$ = 9.5 kcal mol^{-1} was calculated for removal of an acetonitrile molecule from ^{3}**1**$_{AN}$.

To understand the reactivity differences of ^{3}**1** and ^{3}**1**$_{AN}$ on the one hand with iron(IV)-oxo porphyrin cation radical and nonheme iron(IV)-oxo models, on the other hand, we set up a valence bond/molecular orbital diagram on the orbital forming and breaking processes that take place during the rate determining step of the reaction. In particular, we recently proposed a two-parabola model to predict barrier heights of oxygen atom transfer reactions,[36] see right-hand-side of Figure 5 for details. This model considers the reactants and products to reside in the minimum point of a parabola at a reaction coordinate x = 0 (reactants, **R**) and x = 1 (products). The two parabolas cross in a point just above the actual transition state at a reaction coordinate of x = ½ and the energy of the crossing point (ΔE_{cross}) can then be described from the two parabola functions (y_R and y_P). Specifically, we derived previously that the energy at the crossing point is a function of the driving force from reactants to products (ΔE_{rp}) and the Franck-Condon energy between the two curves at x = 0 ($E_{FC,\mathbf{R}}$), Eq 1.

$$\Delta E_{cross} = \frac{1}{4} E_{FC,\mathbf{R}} + \frac{3}{4} \Delta E_{rp} \qquad (1)$$

The actual transition state is located slightly below the crossing point and using valence bond modelling Shaik[37] predicted that it is lower by a contribution due to the resonance energy B. It was further estimated that B is one half of the weakest bond that is either broken or formed during a hydrogen atom abstraction reaction.

For the oxidants reported in Table 1, we estimated the crossing point for hydrogen atom abstraction from propene and consequently the barrier height ($\Delta E^{\ddagger}_{VB,H,Pr}$) from empirical values. Figure 5 also shows the relevant bonding orbitals in Lewis structures along the hydrogen atom abstraction pathway by ^{3}**1** (top left) and ^{4}[Fe^{IV}(O)(Por$^{+\bullet}$)SCys] (bottom left) as a model of P450 Compound I. Thus, upon hydrogen atom abstraction the substrate C–H orbital (σ_{CH}) needs to be broken into atomic orbitals ($2p_C$ and $1s_H$) and the $1s_H$ then forms a new O–H orbital (σ_{OH}) with a $2p_O$ atomic orbital on the oxo group. This atomic $2p_O$ orbital originates from the π_{xz}/π^*_{xz} pair of orbitals along the Fe–O bond that is split back into atomic orbitals. As the π_{xz}/π^*_{xz} pair of orbitals is occupied with three electrons, after breaking these bonds one electron stays on oxygen ($2p_O$), while the other two move to the iron: One electron occupies the now non-bonding $3d_{xz}$ orbital, whereas the other electron is transferred into the σ^*_{z2} orbital.

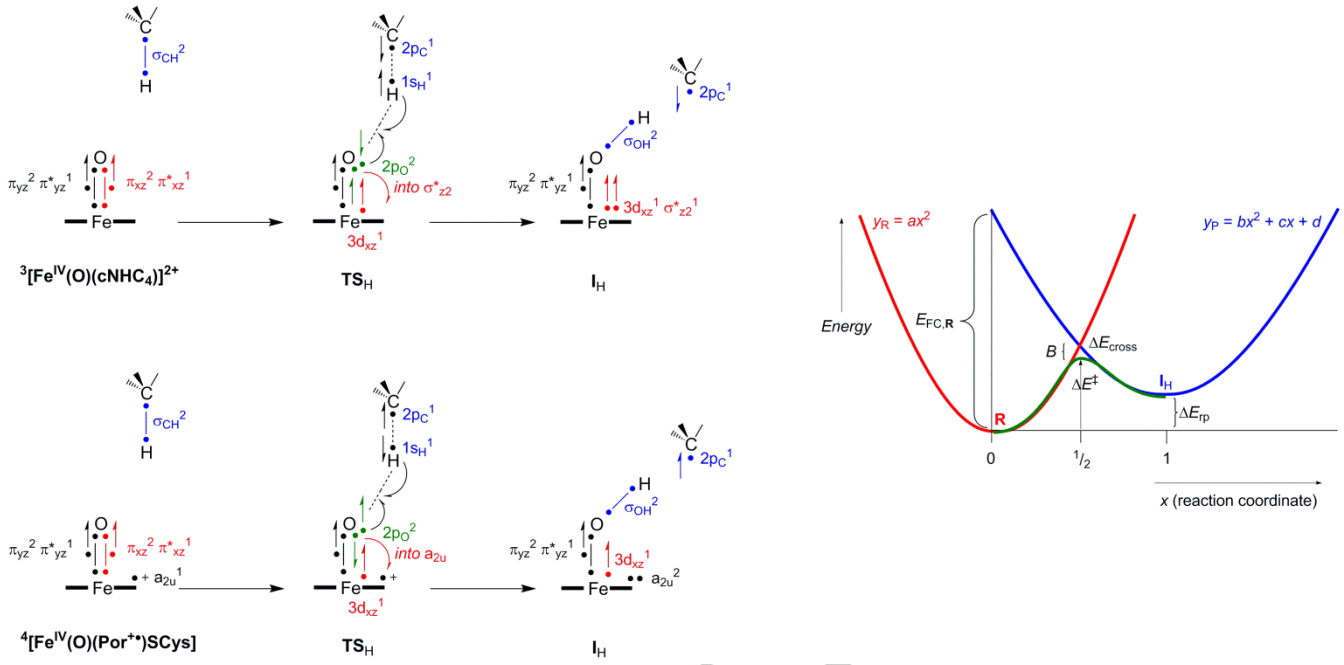

Figure 5. Electron distribution over key orbitals during the hydrogen atom abstraction process in ^{3}**1** (top) and ^{4}[Fe^{IV}(O)(Por$^{+\bullet}$)(SCys)] (bottom). A line with two dots represents a bonding orbital with two electrons.

Table 3. Calculated intrinsic properties of oxidants and predicted and DFT calculated propene hydrogen atom abstraction barriers.

Oxidant[a]	EA	BDE$_{OH}$ [b]	E_{π/π^*xz}	E_{Exc}	$\Delta E^{\ddagger}_{VB,H,Pr}$	$\Delta E^{\ddagger}_{DFT,H,Pr}$
^{3}**1**	87.9	84.0	99.1	134.2	15.3	15.2
^{3}**1**$_{AN}$	77.1	77.2	95.6	154.9	26.4	21.2
^{4}[Fe(O)(Por$^{+\bullet}$)(SH)]	114.2	83.2	83.1	108.4	5.6	17.1
^{3}[Fe(O)(N4Py)]$^{2+}$	93.3	83.0	84.5	163.3	19.9	20.7

[a] All values are in kcal mol^{-1} and include ZPE and solvent corrections. [b] Adiabatic value.

Therefore, the orbital processes that happen in the hydrogen atom abstraction by ^{3}**1** are: (1) The breaking of the σ_{CH} orbital into atomic orbitals, (2) The formation of a σ_{OH} orbital from atomic orbitals, (3) The breaking of the π_{xz}/π^*_{xz} pair of orbitals into atomic orbitals, and (4) The excitation of an electron from $3d_{xz}$ to σ^*_{z2}. As such, the Franck-Condon energy ($E_{FC,1}$)in the reactants for the hydrogen atom abstraction by ^{3}**1** can be described by Eq 2. In this equation the breaking of the π_{xz}/π^*_{xz} pair of orbitals is given as E_{π/π^*xz} and the excitation energy from $3d_{xz}$ to σ^*_{z2} is $E_{Exc,xz\rightarrow\sigma^*zz}$. Finally, the bond dissociation energies of the C–H bond of the substrate and the O–H bond of the iron(III)-hydroxo product are described by BDE_{CH} and BDE_{OH}, respectively. We estimated the π_{xz}/π^*_{xz} energy gap and the π_{xz} to σ^*_{z2} excitation energy from the individual molecular orbitals in the reactant complexes and give the obtained values in Table 3. In addition, we calculated the BDE_{OH} values from the difference in energy between the iron(III)-hydroxo complex and the sum of the iron(IV)-oxo and a hydrogen atom and also present the electron affinity (EA) of the complexes in Table 3.

$$E_{FC,1} = E_{\pi/\pi^*xz} + E_{Exc,xz\rightarrow\sigma^*zz} + BDE_{CH} - BDE_{OH} \qquad (2)$$

The driving force for the hydrogen atom abstraction is simply taken as the difference in energy between BDE_{CH} and BDE_{OH}. Indeed, a difference of –2.1 kcal mol^{-1} is found, which is almost identical to the value of the radical intermediate from isolated reactants (see Figure 4). The VB model predicts hydrogen atom abstraction barriers of 15.3 (propene) and 15.1 (ethylbenzene) kcal mol^{-1} from empirical values. These values are in excellent agreement with the DFT barriers reported in Figure 4 and confirm the individual electronic components that contribute to the hydrogen atom abstraction barrier.

Addition of an axial acetonitrile ligand to form ^{3}**1**$_{AN}$ has a dramatic effect on the hydrogen atom abstraction barriers and leads to a VB predicted barrier of 26.4 kcal mol^{-1}, which is in

reasonable agreement with the DFT result from Table 1. The reason the barriers go up in energy is mostly due to a considerable increase of the $\pi_{xz} \rightarrow \sigma^*_{z2}$ excitation energy. Thus, addition of an axial ligand lowers the metal into the plane of the four carbene atoms, which affects the σ^*_{z2} orbital dramatically and raises it in energy by more than 20 kcal mol^{-1}. In addition, there are further destabilizing effects of the **TS**$_H$ as a result of a smaller BDE_{OH} value, which of course, also affects the driving force. Therefore, binding an axial solvent molecule to ^{3}**1** reduces the oxidative power of the system and makes it a weaker oxidant as an electron is transferred into a higher energy orbital.

Using the same model, as reported previously,[32] the same model can be applied to hydrogen atom abstraction by P450 CpdI. The Franck-Condon value for CpdI is described in a similar way as that for ^{3}**1** and ^{3}**1**$_{AN}$ and depends as well on the π_{xz}/π^*_{xz} energy gap, the BDE_{CH} and BDE_{OH} values, Eq 3. In addition, the excitation energy from π_{xz} is into the a_{2u} orbital, which is much lower in energy than σ^*_{z2} and should cost lesser energy. Consequently, this lower excitation will lead to a reduction in the Franck-Condon energy, although other components may balance it.

$$E_{FC,\mathbf{1}} = E_{\pi/\pi^*xz} + E_{Exc,xz\rightarrow a2u} + BDE_{CH} - BDE_{OH} \qquad (3)$$

As seen from the data in Table 3, VB predicts a low barrier for hydrogen atom abstraction from propene, which is somewhat lower than the DFT calculated value probably because the pairing energy of the two electrons in a_{2u} is not included in the model. Nevertheless, the trend is reproduced well and highlights the components contributing to the hydrogen atom abstraction barrier.

In summary, the VB/MO modelling highlights the key intrinsic properties of the oxidants that drive hydrogen atom abstraction reactions and show that a lower lying orbital is filled by P450 CpdI as compared by the nonheme iron(IV)-oxo analogs. However, the electron affinity of the CpdI model is significantly higher than those of the tetra-cyclic NHC complexes **1** and **1**$_{AN}$.

Conclusions

In this work we report a computational study on substrate hydroxylation and epoxidation of four model substrates by a set of iron(IV)-oxo complexes. In particular, two iron(IV)-oxo complexes with tetra-cyclic NHC ligand system were investigated with and without an axial acetonitrile ligand. The work is compared with reactivity of P450 CpdI and a nonheme iron(IV)-oxo complex with pentadentate N4Py ligand system. The work shows that the pentacoordinate system **1** is an excellent oxidant of olefin epoxidation and aliphatic hydroxylation reactions and reacts with rate determining barriers that are similar to those found for P450 CpdI models. Addition of an axial ligand, however, reduces the activity and raises the barriers dramatically in energy, although they are low enough to take place at room temperature. The differences are analyzed by molecular orbital and valence bond methods and shown to originate from differences in molecular orbital energy levels. Specifically, the σ^*_{z2} orbital is raised from ^{3}**1** to ^{3}**1**$_{AN}$ and is the dominant reason for the slowing down of the reaction. By contrast, P450 CpdI has a lower lying a_{2u} orbital that is accessible and thereby enjoys lower barriers for hydrogen atom abstraction. Overall, the tetra-cyclic NHC ligated iron(IV)-oxo complex is a unique chemical system with reactivity patterns at par with porphyrin complexes. Moreover, the $[Fe^{IV}(O)(cNHC)_4]^{2+}$ complex has well separated triplet and quintet spin state surfaces, whereby the quintet is so much higher in energy that it cannot take a role in catalysis. As such this system enables for spin-selective studies on triplet spin states in oxygen atom transfer reactions.

Experimental Section

Computational methods and procedures follow previously described studies from our group[38] and utilize density functional theory methods as implemented and run in the Gaussian-09 software package.[39] All structures described here are the result of a full geometry optimization (without constraints) with the unrestricted B3LYP hybrid density functional methodology.[40] Although, the initial structures were optimized in the gas-phase, we followed up our studies with full geometry optimizations using a self-consistent reaction-field (SCRF) model with a dielectric constant mimicking acetonitrile.[41] In previous work we showed that this model matches experimental structures and reaction mechanisms and rate constants better than gas-phase geometry optimizations, particularly since the system has an overall charge of +2.[16] Details of the gas-phase results are given in the Supporting Information, while we focus here on the solvent corrected data only. Geometry optimizations use an LANL2DZ (+ core potential) on iron and 6-31G* on all other atoms: basis set BS1.[42] Single point energy calculations on the optimized geometries were done with a more elaborate LACV3P+ (+ core potential) basis set on iron and 6-311+G* on the rest of the atoms: basis set BS2, including the implicit solvation model. Vibrational frequencies reported here are unscaled.

We created a tetra-cyclic-NHC ligand from a porphyrin analogue by replacing carbon and nitrogen atoms and adding hydrogens. Iron(IV)-oxo was then inserted into the ligand to create $[Fe^{IV}(O)(cNHC_4)]^{2+}$ or **1**. Complex **1** was investigated in the triplet and quintet spin states with and without an axial acetonitrile molecule bound. Subsequently, the reactivity in oxygen atom transfer, i.e. double bond epoxidation and C–H hydroxylation, was studied with styrene, propene (hydroxylation and epoxidation) and ethylbenzene.

Kinetic isotope effects for the replacement of hydrogen atoms by deuterium were initially calculated using the Eyring equation (KIE_E) by taking the free energy of activation ($\Delta G^{\ddagger}$) difference of the systems with all hydrogen atoms and the structure where one or more hydrogen atoms were replaced by deuterium atoms.[29,43] The free energy difference was then converted into a rate constant ratio (k_H/k_D) by taking the natural logarithm over the free energy difference divided by the gas constant (R) and the temperature (T = 298K), Eq 4.

$$KIE_E = \exp\{(\Delta G^{\ddagger}_D - \Delta G^{\ddagger}_H)/RT\} \qquad (4)$$

The effect of tunnelling on the kinetic isotope effects was calculated from the Wigner correction to the KIE_E by multiplication with the tunnelling ratio (Q_{tH}/Q_{tD}) taken from the change in imaginary frequency (ν) in the transition state, Eqs 5 and 6.

$$KIE_W = KIE_E \times Q_{tH}/Q_{tD} \qquad (5)$$

$$Q_t = 1 + \frac{1}{24}\left(\frac{h\nu}{kT}\right)^2 \qquad (6)$$

In Eq 6, k is the Boltzmann constant and h is Planck's constant.

Mössbauer parameters were calculated in Orca for ^{3}**1** and ^{3}**2** on the B3LYP/BS1 optimized geometries.[44] These calculations use approaches discussed before[45] with the unrestricted B3LYP employed with basis set CP(PPP) with effective core potential on iron and SV(P) on the rest of the atoms.

Acknowledgements

FGCR thanks the Conacyt Mexico for a studentship.

Keywords: iron(IV)-oxo • epoxidation • hydroxylation • NHC • density functional theory

[1] a) P. R. Ortiz de Montellano, *Annu. Rev. Pharmacol. Toxicol*. **1992**, *32*, 89–107; b) E. L. Raven, *Nat. Prod. Rep*. **2003**, *20*, 367–381; c) T. L. Poulos, *Arch. Biochem. Biophys*. **2010**, *500*, 3–12; d) F. Hollmann, I. W. C. E. Arends, K. Buehler, A. Schallmey, B. Bühler, *Green Chemistry* **2011**, *13*, 226–265.

[2] a) P. Nicholls, I. Fita, P. C. Loewen, *Adv. Inorg. Chem*. **2000**, *51*, 51–106; b) N. G. Veitch, A. T. Smith, *Adv. Inorg. Chem*. **2000**, *51*, 107–162; c) H.-P. Hersleth, U. Ryde, P. Rydberg, C. H. Görbitz, K. K. Andersson, *J. Inorg. Biochem*. **2006**, *100*, 460–476.

[3] a) M. Sono, M. P. Roach, E. D. Coulter, J. H. Dawson, *Chem. Rev*. **1996**, *96*, 2841–2888; b) J. T. Groves, *Proc. Natl. Acad. Sci. USA*, **2003**, *100*, 3569–3574; c) P. R. Ortiz de Montellano (Ed.) *Cytochrome P450: Structure, Mechanism and Biochemistry*. 3rd ed., Kluwer Academic/Plenum Publishers, New York, 2004; d) I. G. Denisov, T. M. Makris, S. G. Sligar, I. Schlichting, *Chem. Rev*. **2005**, *105*, 2253–2277; e) B. Meunier, S. P. de Visser, S. Shaik, *Chem. Rev*. **2004**, *104*, 3947–3980; f) K. M. Kadish, K. M. Smith and R. Guilard (Eds.) *Handbook of Porphyrin Science*. World Scientific: New Jersey, 2010; g) P. R. Ortiz de Montellano, *Chem. Rev*. **2010**, *110*, 932–948.

[4] a) J. H. Dawson, *Science* **1988**, *240*, 433–439; b) I. Schlichting, J. Berendzen, K. Chu, A. M. Stock, S. A. Maves, D. E. Benson, R. M. Sweet, D. Ringe, G. A. Petsko, S. G. Sligar, *Science* **2000**, *287*, 1615–1622; c) S. Shaik, D. Kumar, S. P. de Visser, A. Altun, W. Thiel, *Chem. Rev*. **2005**, *105*, 2279–2328.

[5] a) J. E. Roberts, B. M. Hoffman, R. Rutter, L. P. Hager, *J. Am. Chem. Soc*. **1981**, *103*, 7654–7656; b) M. Sivaraja, D. B. Goodin, M. Smith, B. M. Hoffman, *Science* **1989**, *245*, 738–740; c) D. B. Goodin, D. E. McRee, *Biochemistry* **1993**, *32*, 3313–3324.

[6] J. Rittle, M. T. Green, *Science* **2010**, *330*, 933–937.

[7] J. H. Dawson, R. H. Holm, J. R. Trudell, G. Barth, R. E. Linder, E. Bunnenberg, C. Djerassi, *J. Am. Chem. Soc*. **1976**, *98*, 3707–3709.

[8] a) M. Costas, M. P. Mehn, M. P. Jensen, L. Que, Jr., *Chem. Rev*. **2004**, *104*, 939–986; b) P. C. A. Bruijnincx, G. van Koten, R. J. M. Klein Gebbink, *Chem. Soc. Rev*. **2008**, *37*, 2716–2744; c) M. M. Abu-Omar, A. Loaiza, N. Hontzeas, *Chem. Rev*. **2005**, *105*, 2227–2252; d) L. Que Jr, *Acc. Chem. Res*. **2007**, *40*, 493–500; e) W. Nam, *Acc. Chem. Res*. **2007**, *40*, 522–531; f) M. Atanasov, P. Comba, S. Hausberg, Martin, *Coord. Chem. Rev*. **2009**, *253*, 2306–2314.

[9] a) I. Aviv-Harel, Z. Gross, *Coord. Chem. Rev*. **2011**, *255*, 717–736; b) K. E. Thomas, A. B. Alemayehu, J. Conradie, C. M. Beavers, A. Ghosh, *Acc. Chem. Res*. **2012**, *45*, 1203–1214; c) M. M. Abu-Omar, *Dalton Trans*. **2011**, *40*, 3435–3444.

[10] H. M. Neu, R. A. Baglia, D. P. Goldberg, *Acc. Chem. Res*. **2015**, *48*, 2754–2764.

[11] a) P. Afanasiev, A. B. Sorokin, *Acc. Chem. Res*. **2016**,*49*, 583–593; b) Ü. İşci, A. S. Faponle, P. Afanasiev, F. Albrieux, V. Briois, V. Ahsen, F. Dumoulin, A. B. Sorokin, S. P. de Visser, *Chem. Sci*. **2015**, *6*, 5063–5075.

[12] a) M. N. Hopkinson, C. Richter, M. Schedler, F. Glorius, *Nature* **2014**, *510*, 485–496; b) D. M. Flanigan, F. Romanov-Michailidis, N. A. White, T. Rovis, *Chem. Rev*. **2015**, *115*, 9307–9387; c) D. Domyati, S. L. Hope, R. Latifi, M. D. Hearns, L. Tahsini, *Inorg. Chem*. **2016**, *55*, 11685–11693.

[13] a) M. R. Anneser, S. Haslinger, A. Pöthig, M. Cokoja, J.-M. Basset, F. E. Kühn, *Inorg. Chem*. **2015**, *54*, 3797–3804; b) M. R. Anneser, S. Haslinger, A. Pöthig, M. Cokoja, V. D'Elia, M. P. Högerl, J.-M. Basset, F. E. Kühn, *Dalton Trans*. **2016**, *45*, 6449–6455.

[14] S. Ye, C. Kupper, S. Meyer, E. Andris, R. Navrátil, O. Krahe, B. Mondal, M. Atanasov, E. Bill, J. Roithová, F. Meyer, F. Neese, *J. Am. Chem. Soc*. **2016**, *138*, 14312–14325.

[15] See, e.g., a) F. Ogliaro, N. Harris, S. Cohen, M. Filatov, S. P. de Visser, S. Shaik, *J. Am. Chem. Soc*. **2000**, *122*, 8977–8989; b) T. Kamachi, K. Yoshizawa, *J. Am. Chem. Soc.* **2003**, *125*, 4652–4661; c) D. Li, Y. Wang, K. Han, *Coord. Chem. Rev*. **2012**, *256*, 1137–1150.

[16] a) F. G. Cantú Reinhard, A. S. Faponle, S. P. de Visser, *J. Phys. Chem. A* **2016**, *120*, 9805–9816; b) T. Yang, M. G. Quesne, H. M. Neu, F. G. Cantú Reinhard, D. P. Goldberg, S. P. de Visser, *J. Am. Chem. Soc*. **2016**, *138*, 12375–12386.

[17] a) D. Balcells, C. Raynaud, R. H. Crabtree, O. Eisenstein, *Inorg. Chem*. **2008**, *47*, 10090–10099. b) S. P. de Visser, J.-U. Rohde, Y.-M. Lee, J. Cho, W. Nam, *Coord. Chem. Rev*. **2013**, *257*, 381–393; c) D. Wang, K. Ray, M. J. Collins, E. R. Farquhar, J. R. Frisch, L. Gómez, T. A. Jackson, M. Kerscher, A. Waleska, P. Comba, M. Costas, L. Que Jr, *Chem. Sci.* **2013**, *4*, 282–291.

[18] a) J.-U. Rohde, J.-H. In, M. H. Lim, W. W. Brennessel, M. R. Bukowski, A. Stubna, E. Münck, W. Nam, L. Que Jr, *Science* **2003**, *299*, 1037-1039; b) M. Martinho, F. Banse, J.-F. Bartoli, T. A. Mattioli, P. Battioni, O. Horner, S. Bourcier, J.-J. Girerd, *Inorg. Chem*. **2005**, *44*, 9592–9596; c) A. S. Borovik, *Acc. Chem. Res*. **2005**, *38*, 54–61.

[19] a) D. Kumar, H. Hirao, L. Que Jr., S. Shaik, *J. Am. Chem. Soc*. **2005**, *127*, 8026–8027; b) S. P. de Visser, *J. Am. Chem. Soc*. **2006**, *128*, 9813–9824; c) F. Banse, J.-J. Girerd, V. Robert, *Eur. J. Inorg. Chem*. **2008**, 4786–4791; d) C. Y. Geng, S. F. Ye, F. Neese, *Angew. Chem. Int. Ed*. **2010**, *49*, 5717–5720.

[20] A. Rosa, G. Ricciardi, G. *Inorg. Chem*. **2012**, *51*, 9833–9845.

[21] a) M. L. Neidig, A. Decker, O. W. Choroba, F. Huang, M. Kavana, G. R. Moran, J. B. Spencer, E. I. Solomon, *Proc. Natl. Acad. Sci. USA*. **2006**, *103*, 12966–12973; b) H. Hirao, D. Kumar, L. Que Jr., S. Shaik, *J. Am. Chem. Soc*. **2006**, *128*, 8590–8606.

[22] S. P. de Visser, *J. Am. Chem. Soc*. **2010**, *132*, 1087–1097.

[23] D. Kumar, B. Karamzadeh, G. N. Sastry, S. P. de Visser, *J. Am. Chem. Soc*. **2010**, *132*, 7656–7667.

[24] D. Kumar, R. Latifi, S. Kumar, E. V. Rybak-Akimova, M. A. Sainna, S. P. de Visser, *Inorg. Chem*. **2013**, *52*, 7968–7979.

[25] a) L. Bernasconi, E.-J. Baerends, *Eur. J. Inorg. Chem.* **2008**, 1672–1681; b) S. D. Wong, C. B. Bell III, L. V. Liu, Y. Kwak, J. England, E. E. Alp, J. Zhao, L. Que Jr, E. I. Solomon, *Angew. Chem. Int. Ed*. **2011**, *50*, 3215–3218; *Angew. Chem.* **2011**, *123*, 3273–3276; c) S. Sahu, L. R. Widger, M. G. Quesne, S. P. de Visser, H. Matsumura, P. Moënne-Loccoz, M. A. Siegler, D. P. Goldberg, *J. Am. Chem. Soc*. **2013**, *135*, 10590–10593.

[26] a) S. P. de Visser, *J. Am. Chem. Soc*. **2006**, *128*, 15809–15818; b) S. F. Ye, F. Neese, *Proc. Natl. Acad. Sci. USA* **2011**, *108*, 1228–1233; c) R. Latifi, M. A. Sainna, E. V. Rybak-Akimova, S. P. de Visser, *Chem. Eur. J.* **2013**, *19*, 4058–4068.

[27] a) S. P. de Visser, F. Ogliaro, S. Shaik, *Angew. Chem. Int. Ed*. **2001**, *40*, 2871–2874; b) S. P. de Visser, D. Kumar, S. Shaik, *J. Inorg. Biochem.* **2004**, *98*, 1183–1193.

[28] a) A. Company, L. Gómez, M. Güell, X. Ribas, J. M. Luis, L. Que Jr, M. Costas, *J. Am. Chem. Soc*. **2007**, *129*, 15766–15767; b) J. Park, Y.-M. Lee, W. Nam, S. Fukuzumi, *J. Am. Chem. Soc.* **2013**, *135*, 5052–5061.

[29] a) S. P. de Visser, *Chem. Eur. J*. **2006**, *12*, 8168–8177; b) D. Mandal, S. Shaik, *J. Am. Chem. Soc*. **2016**, *138*, 2094–2097.

[30] See, e.g., a) D. Kumar, G. N. Sastry, S. P. de Visser, *Chem. Eur. J.* **2011**, *17*, 6196–6205; b) L. Ji, A. S. Faponle, M. G. Quesne, M. A. Sainna, J. Zhang, A. Franke, D. Kumar, R. van Eldik, W. Liu, S. P. de Visser, *Chem. Eur. J*. **2015**, *21*, 9083–9092.

[31] a) A. K. Vardhaman, P. Barman, S. Kumar, C. V. Sastri, D. Kumar, S. P. de Visser, *Angew. Chem. Int. Ed*. **2013**, *52*, 12288–12292; b) S. Kumar, A. S. Faponle, P. Barman, A. K. Vardhaman, C. V. Sastri, D. Kumar, S. P. de Visser, *J. Am. Chem. Soc*. **2014**, *136*, 17102–1711.

[32] M. G. Quesne, D. Senthilnathan, D. Singh, D. Kumar, P. Maldivi, A. B. Sorokin, S. P. de Visser, *ACS Catal*. **2016**, *6*, 2230–2243.
[33] D. Kumar, L. Tahsini, S. P. de Visser, H. Y. Kang, S. J. Kim, W. Nam, *J. Phys. Chem. A* **2009**, *113*, 11713–11722.
[34] a) L. Bernasconi, E. J. Baerends, *J. Am. Chem. Soc*. **2013**, *135*, 8857–8867; b) M. A. Sainna, S. Kumar, D. Kumar, S. Fornarini, M. E. Crestoni, S. P. de Visser, *Chem. Sci*. **2015**, *6*, 1516–1529.
[35] a) C. V. Sastri, M. S. Seo, M. J. Park, K. M. Kim, W. Nam, *Chem. Commun*. **2005**, 1405–1407; b) C. V. Sastri, J. Lee, K. Oh, Y. J. Lee, J. Lee, T. A. Jackson, K. Ray,H. Hirao, W. Shin, J. A. Halfen, J. Kim, L. Que Jr, S. Shaik, W. Nam, *Proc. Natl. Acad. Sci. USA* **2007**, *104*, 19181–19186; c) Y. Mekmouche, S. Ménage, C. Toia-Duboc, M. Fontecave, J.-B. Galey, C. Lebrun, J. Pécaut, *Angew. Chem. Int. Ed*. **2001**, *40*, 949–952; d) T. Kurahashi, M. Hada, H. Fujii, *J. Am. Chem. Soc.* **2009**, *131*, 12394–12405.
[36] a) P. Barman, P. Upadhyay, A. S. Faponle, J. Kumar, S. S. Nag, D. Kumar, C. V. Sastri, S. P. de Visser, *Angew. Chem. Int. Ed*. **2016**, *55*, 11091–11095; b) F. G. Cantú Reinhard, M. A. Sainna, P. Upadhyay, G. A. Balan, D. Kumar, S. Fornarini, M. E. Crestoni, S. P. de Visser, *Chem. Eur. J*. **2016**, *22*, 18608–18619.
[37] a) S. S. Shaik, *J. Am. Chem. Soc*. **1981**, *103*, 3692–3701; b) S. Shaik, *Phys. Chem. Chem. Phys*. **2010**, *12*, 8706–8720.
[38] S. P. de Visser, M. G. Quesne, B. Martin, P. Comba, U. Ryde, *Chem. Commun*. **2014**, *50*, 262–282.
[39] M. J. Frisch, *Gaussian* 09, revision D.01; Gaussian, Inc., Wallingford, CT, 2004.
[40] a) A. D. Becke, *J. Chem. Phys*. **1993**, *98*, 5648–5652; b) C. Lee, W. Yang, R. G. Parr, *Phys. Rev. B* **1988**, *37*, 785–789.
[41] J. Tomasi, B. Mennucci, R. Cammi,. *Chem. Rev* **2005**, *105*, 2999–3093.
[42] a) P. J. Hay, W. R. Wadt, *J. Chem. Phys*. **1985**, *82*, 270–283; b) W. J. Hehre, R. Ditchfield, J. A. Pople, *J. Chem. Phys*. **1972**, *56*, 2257–2261.
[43] D. Kumar, S. P. de Visser, S. Shaik, *J. Am. Chem. Soc*. **2004**, *126*, 5072–5073.
[44] F. Neese, ORCA; 2.9 ed. Bonn, Germany, 2009.
[45] E. P. Tchesnokov, A. S. Faponle, C. G. Davies, M. G. Quesne, R. Turner, M. Fellner, R. J. Souness, S. M. Wilbanks, S. P. de Visser, G. N. L. Jameson, *Chem. Commun*. **2016**, *52*, 8814–8817.

Entry for the Table of Contents

FULL PAPER

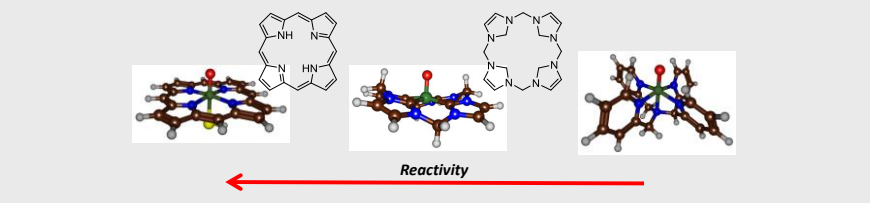

A density functional theory study on a nonheme iron(IV)-oxo complex with tetracyclic NHC ligand system is reported. The work shows that it is an efficient oxidant of substrate epoxidation and hydroxylation reactions in the absence of an axial ligand. The results have been analysed with valence bond and molecular orbital diagrams and compare the reactivity with heme and nonheme iron(IV)-oxo complexes.

*Fabián G. Cantú Reinhard,[a] and Sam P. de Visser**

Page No. – Page No.

Oxygen atom transfer using an iron(IV)-oxo embedded in a tetracyclic N-heterocyclic carbene system: How does the reactivity compare to Cytochrome P450 Compound?